ASM | Applied and Environmental Microbiology

| Editor's Pick | Host-Microbial Interactions | Full-Length Text

Tick cells as a tractable arthropod model for studying *Orientia tsutsugamushi*

Magda A. Rogowska-van der Molen,[1] Filomena Gallo,[2] Lesley Bell-Sakyi,[3] Jeanne Salje[1,4,5]

AUTHOR AFFILIATIONS See affiliation list on p. 14.

Downloaded from https://journals.asm.org/journal/aem on 12 June 2026 by 81.101.145.98.

ABSTRACT *Orientia tsutsugamushi* (*Ot*), the causative agent of scrub typhus, is an obligate intracellular bacterium naturally maintained in *Leptotrombidium* mites, yet its interactions within arthropod hosts remain poorly understood. Here, we employed two tick cell lines, *Ixodes scapularis* ISE6 and *Rhipicephalus microplus* BME/CTVM23, as arthropod models to investigate the intracellular lifecycle of *Ot* strains TA686 and Karp. Both strains efficiently infected tick cells and replicated within them, with ISE6 supporting more robust growth. Electron microscopy images revealed that *Ot* maintains its characteristic cytoplasmic, non-vacuolar location in tick cells and exits infected cells by budding off the surface in a membrane-encased structure. Time-course immunofluorescence imaging demonstrated progressive intracellular replication and dynamic expression of *Ot* outer membrane autotransporters ScaA and ScaC, with ScaC enriched early in infection and ScaA at later stages. A microscopy-based analysis of metabolic activity using a clickable methionine analog L-homopropargylglycine showed that high ScaA abundance correlated with reduced translational activity, suggesting a link between ScaA abundance and late-stage or extracellular-like developmental states. The subcellular location of *Ot* in tick cells differs from the characteristic dynein-driven perinuclear clustering observed in mammalian cells and was not sensitive to disruption of microtubules, suggesting a distinct mode of distribution. Together, these findings identify tick cell lines as tractable and biologically relevant arthropod models for studying *Ot* and dissecting host-microbe interactions.

IMPORTANCE *Orientia tsutsugamushi*, the causative agent of scrub typhus, is an obligate intracellular bacterium naturally maintained in trombiculid mites, yet its interactions with arthropod host cells remain poorly understood. This study establishes, for the first time, a tractable *in vitro* arthropod model for *O. tsutsugamushi* using tick cell lines from *Ixodes scapularis* and *Rhipicephalus microplus*. We demonstrate that both virulent and avirulent *Orientia* strains efficiently infect and replicate in these cells while maintaining their characteristic cytoplasmic location and budding mode of exit. Distinct temporal expression of the bacterial autotransporters ScaA and ScaC and their relationship to metabolic activity reveal stage-specific adaptations during infection. These findings provide essential mechanistic insight into how *O. tsutsugamushi* persists and develops within arthropod hosts. The tick cell model enables comparative studies of host-pathogen interactions across vector species and offers a powerful tool to investigate transmission biology and potential targets for intervention.

KEYWORDS *in vitro* arthropod model, host-pathogen interactions, *Orientia tsutsugamushi*, *Rickettsiales*, scrub typhus, tick cell line

Orientia tsutsugamushi (*Ot*) is an obligate intracellular gram-negative bacterium in the order Rickettsiales found in the salivary glands and ovaries of *Leptotrombidium* mites. Chigger mites are the primary arthropod reservoir and vector of *Ot*, and the

Editor Pablo Tortosa, Universite de la Reunion, Ste Clotilde, France

Address correspondence to Jeanne Salje, jss53@cam.ac.uk.

The authors declare no conflict of interest.

See the funding table on p. 14.

Received 27 December 2025
Accepted 20 May 2026
Published 12 June 2026

Copyright © 2026 Rogowska-van der Molen et al. This is an open-access article distributed under the terms of the Creative Commons Attribution 4.0 International license.

Downloaded from https://journals.asm.org/journal/aem on 12 June 2026 by 81.101.145.98.

bacteria are maintained through mite generations by transovarial transmission. When the infected chigger larvae feed on humans, the bacteria can enter through the skin and cause the disease scrub typhus (1–3). This life-threatening condition causes one of the most severe rickettsial diseases in humans, with a median mortality rate of 6% if left untreated (4, 5). Scrub typhus is a leading cause of severe febrile illness in many rural parts of Asia, a region containing two-thirds of the world's population. Moreover, recent reports of scrub typhus from Latin America, the Middle East, and Africa suggest that the disease is distributed more globally than previously recognized (6–8).

The two most well-studied families in the Rickettsiales are the Anaplasmataceae and Rickettsiaceae (9). The former includes *Anaplasma* spp. and *Ehrlichia* spp. that reside within membrane-bound vacuoles inside host cells and are released primarily through exocytosis-like mechanisms or within vesicles, although host cell lysis may also occur (10). The latter includes *Rickettsia* spp. and *Orientia* spp. that replicate directly in the eukaryotic cytoplasm. The intracellular lifecycle of *Ot* has been studied previously in a range of mammalian cell types (11, 12), where it was discovered that *Ot* enters cells through induced clathrin-mediated endocytosis and macropinocytosis and exits the endolysosomal pathway shortly after entry, where it further replicates freely in the host cytoplasm (13). As an obligate intracellular bacterium, *Ot* has lost the ability to synthesize many essential metabolites, such as amino acids, nucleotides, and cofactors, making it entirely dependent on host-derived resources to sustain its intracellular growth (14, 15). In mammalian cells, *Ot* typically traffics to the perinuclear region using dynein-dependent motility and replicates in a tightly packed microcolony (16). After 3–7 days post-infection, *Ot* traffics to the cell periphery, where it spreads by budding off the surface of infected cells in vesicles surrounded by the host cell membrane (17). These extracellular bacteria (EB) are inactive in terms of replication and protein synthesis but can infect subsequent host cells (17, 18). This lifecycle and transmission route are different from the other studied organisms within the order Rickettsiales.

While significant advances have been made in understanding *Ot* biology in mammalian cells, comparatively little is known about its interaction with arthropod host cells. In its natural lifecycle, *Ot* is maintained in *Leptotrombidium* mites, yet the molecular and cellular basis of this persistence remains largely unexplored. The lack of a robust *in vitro* arthropod model has hindered the investigation of bacterial replication and adaptation mechanisms within vector cells. Tick cell lines have previously proven invaluable for studying vector-borne pathogens, helping to define the complex nature of the host-vector-pathogen interactions, including those involving members of the order Rickettsiales, such as *Rickettsia* and *Ehrlichia* species (19–21). Given the close phylogenetic relationships between ticks and trombiculid mites, and the lack of any established mite cell lines, tick cell cultures offer a surrogate model to investigate *Ot* growth in arthropod cells.

In this study, we used the virulent Karp strain, a well-characterized human clinical isolate, together with the avirulent TA686 strain, which has been reported to lack virulence in murine and non-human primate infection models (22), to examine bacterial development within two tick cell lines, ISE6 (23) and BME/CTVM23 (24). By establishing this system, we aimed to provide a new experimental framework to study the vector stage of *Ot* biology. We compared the two strains in phylogenetically distinct tick cell lines to assess their *in vitro* growth properties and metabolic activity and characterized the intracellular lifecycle using immunofluorescence microscopy (IFM). Altogether, our findings suggest that tick cells represent a promising arthropod model for investigating *Ot* cell biology.

MATERIALS AND METHODS

Tick cell lines

The *Ixodes scapularis* embryo-derived cell line ISE6 (23) was maintained at 32°C in L-15B300 medium (25) supplemented with 10% tryptose phosphate buffer (TPB), 10% fetal bovine serum (FBS; Thermo Scientific), 2 mM L-glutamine (Sigma-Aldrich), and 0.1% bovine lipoprotein concentrate (MP Biomedicals). The *Rhipicephalus microplus* embryo-derived cell line BME/CTVM23 (24) was maintained at 32°C in L-15 (Leibovitz) medium supplemented with 10% TPB, 20% FBS, and 2 mM L-glutamine. Culture media were supplemented with 100 U/mL penicillin and 100 µg/mL streptomycin (Sigma-Aldrich). Both cell lines were grown in 2.2 mL volumes in flat-sided cell culture tubes (Nunc) with weekly medium changes and were split every 2 weeks as described previously (26).

Bacterial propagation

Ot strains TA686 and Karp were propagated in the mouse fibroblast cell line NCTC clone 929 (L929) purchased from ATCC (catalog no. CCL-1) following a previously described protocol (27). Briefly, L929 cells were seeded in T75 flasks at a density of 3×10^6 cells per flask and incubated overnight before infection. A frozen bacterial stock was thawed and added directly to the flasks. On day 6 post-infection, the medium was removed, followed by washing with phosphate-buffered saline (PBS; Gibco) once, and the cells were then scraped from the flask. The cells were resuspended in plain Dulbecco's modified Eagle medium (DMEM; Thermo Scientific), transferred to a 2 mL Safe-Lock tube, and homogenized using a bead-mill homogenizer (Fisher Scientific, Finland) at a speed of 5 for 1 min. The suspension was then centrifuged at 300 × *g* for 5 min. Supernatant was collected, then centrifuged at 14,000 × *g* for 3 min to pellet the *Ot* bacteria. The bacterial pellet was resuspended in sucrose-phosphate-glutamate buffer and stored at −80°C until use.

In vitro growth in tick cells

Bacteria were added directly to the tick cells in growth media at a multiplicity of infection of 50, determined by measuring the number of bacterial genome equivalents added to a specific number of uninfected cells, and incubated for 24 h. After incubation, the supernatant was removed, and fresh growth medium was added to the inoculated cells. Samples for DNA extraction and IFM were taken by resuspending the cells with a serological pipette. For DNA extraction, 100 µL of cell suspension was added to 900 µL alkaline lysis buffer (25 mM NaOH, 0.2 mM EDTA), and the samples were boiled at 95°C for 30 min to inactivate bacteria. The samples were stored at −20°C until further use. For the IFM, eight-well coverslips (µ-Slide ibiTreat) coated with Concanavalin A (ConA) to support host cells' adhesion to the coverslip surface and prevent their detachment in subsequent immunofluorescence staining were prepared before seeding cells as described previously (28). Briefly, the eight-well ibiTreat was coated with 0.5 mg/mL ConA (AA Blocks, USA) working solution for 30 min at room temperature. Then, each well was rinsed with sterile distilled water and dried for at least 16 h before seeding the cells. A total of 5×10^4 cells/mL were seeded in each well of the eight-well ConA ibidi and incubated at 32°C for 2 h. For the nocodazole assay, ISE6 cells infected with *Ot* strain Karp were treated with either dimethyl sulfoxide (DMSO; control) or 10 µM nocodazole dissolved in DMSO (Sigma Aldrich) for 6 h at 32°C prior to imaging. Then, the samples were fixed with 4% formaldehyde solution ([wt/vol]; Thermo Scientific) for 30 min at room temperature, followed by rinsing three times with PBS. Samples were stored in the dark at 4°C until staining.

Bacterial concentration was quantified by qPCR (27). The primers and TaqMan probe used for the 47 kDa target gene were as follows: forward 5′-TCCAGAATTAAATGAGAATT TAGGAC-3′, reverse 5′-TTAGTAATTACATCTCCAGGAGCAA-3′, and probe 5′-FAM-TTCCACA TTGTGCTGCAGATCCTTC-TAMRA-3′. The qPCR mixture consisted of 1× qPCR Probe Mix LO-ROX (PCR Biosystems, UK), 0.1 µM of each forward and reverse primer, 0.2 µM probe, RT-PCR grade water (Thermo Scientific), and 1 µL of extracted DNA. Real-time PCR was

Downloaded from https://journals.asm.org/journal/aem on 12 June 2026 by 81.101.145.98.

performed on a CFX Duet Thermal Cycler (Bio-Rad, USA) using the following settings: initial denaturation at 95°C for 2 min, followed by 45 cycles of 95°C for 15 s, 60°C for 30 s, with fluorescence acquisition during the 60°C annealing/extension phase. DNA copy numbers were calculated by comparison with a standard curve constructed from a serial dilution of a 47 kDa standard in the range of 10^1–10^7 copies (29).

Scanning electron microscopy and transmission electron microscopy

Ot-infected ISE6 cells at 12 days post-infection and BME/CTVM23 at 19 days post-infection were fixed overnight at 4°C in a solution containing 2% glutaraldehyde and 2% formaldehyde in 0.05 M sodium cacodylate buffer (pH 7.4) supplemented with 2 mM calcium chloride. Following fixation, samples were washed five times with 0.05 M sodium cacodylate buffer (pH 7.4) and post-fixed in a solution of 1% osmium tetroxide and 1.5% potassium ferricyanide in the same buffer for 3 days at 4°C. After five washes in deionized water (DIW), samples were incubated with 0.1% (wt/vol) thiocarbohydrazide in DIW for 20 min at room temperature in the dark. This was followed by five DIW washes and a second osmication step using 2% osmium tetroxide in DIW for 1 h at room temperature. Samples were washed five times again in DIW and block-stained with 2% uranyl acetate in 0.05 M maleate buffer (pH 5.5) for 3 days at 4°C. After a final series of five DIW washes, samples were dehydrated through a graded ethanol series (50%, 70%, 95%, 100%, and 100% dry) and 100% dry acetonitrile, with three exchanges at each step for at least 5 min.

Infiltration was performed overnight in a 1:1 mixture of 100% dry acetonitrile and Quetol resin (without benzyldimethylamine [BDMA]), followed by 3 days in 100% Quetol (without BDMA). Samples were then infiltrated for 5 days in 100% Quetol resin containing BDMA, with daily resin exchanges. The Quetol resin mixture consisted of 12 g Quetol 651, 15.7 g nonenyl succinic anhydride, 5.7 g methyl nadic anhydride, and 0.5 g BDMA (all reagents from TAAB). Samples were embedded and cured at 60°C for 2 days.

For scanning electron microscopy (SEM) imaging, thin sections (~200 nm) were cut using a Leica Ultracut E ultramicrotome, placed on Melinex coverslips, and air dried. Coverslips were mounted on aluminum SEM stubs using conductive carbon tabs, and edges were painted with conductive silver paint. Samples were sputter-coated with 30 nm carbon using a Quorum Q150T E carbon coater. Imaging was performed using a Verios 460 scanning electron microscope (FEI/Thermo Fisher) at 4 keV accelerating voltage and 0.2 nA probe current in backscatter mode, using the concentric backscatter detector in immersion mode at a working distance of 3.5–4 mm. Stitched maps were acquired using FEI MAPS software with the default stitching profile and 5% image overlap.

For transmission electron microscopy (TEM) imaging, ultra-thin sections (~90 nm) were cut and collected on 300 mesh bare copper grids. Samples were imaged using a Tecnai G2 transmission electron microscope (FEI/Thermo Fisher) operated at 200 keV accelerating voltage. A 20 µm objective aperture was used to enhance image contrast. Images were acquired with an AMT digital camera.

Immunofluorescence microscopy

Cells were permeabilized on ice by incubating in absolute ethanol for 30 min, followed by 0.5% Triton X-100 for 30 min. A blocking step was performed at room temperature in the dark using PBS (pH 7.4) containing 1% bovine serum albumin for 30 min. The samples were then incubated at 4°C overnight with an in-house-generated primary antibody, i.e., human and rat monoclonal antibodies against TSA56 for strains TA686 and Karp, respectively, and in-house rabbit polyclonal antibodies against autotransporter proteins ScaA and ScaC (10). β-Tubulin was labeled using a mouse primary antibody (T4026, Sigma-Aldrich). The samples were then incubated with a secondary antibody, i.e., goat-anti-rabbit Alexa Fluor Plus 555 (A32732, Thermo Scientific), goat anti-human Alexa Fluor 488, goat-anti-human Alexa Fluor 647 (A21445, Thermo Scientific), or goat anti-rat Alexa Fluor 488 (A11006, Thermo Scientific) at a dilution of 1:500, supplemented with the nuclear stain 4′,6-diamidino-2-phenylindole (DAPI; 1:1,000; Adva Tech Group Inc.,

Downloaded from https://journals.asm.org/journal/aem on 12 June 2026 by 81.101.145.98.

USA) and plasma membrane with HCS CellMask Deep Red (1:5,000; H32721A, Thermo Scientific) at 37°C for 1 h. Samples were washed with PBS after each immunofluorescence labeling step. Samples were mounted using mounting medium (20 mM Tris, pH 8.0, 0.5% N-propyl-gallate, and 90% glycerol). The levels of TSA56, ScaA, and ScaC expression were scored manually in individual infected cells since the computational segmentation tools were unable to distinguish individual tick cells, which tend to form clumps and aggregates. *Ot* was quantified in each tick cell, and scoring was conducted according to the proportion of the cells expressing TSA56, ScaA, or ScaC. Subsequently, each tick cell was assigned a label, i.e., "sparse" if less than 50% of bacteria expressed the protein, and subsequently "widespread" when 50%–99% expressed the corresponding protein. "Uniform" represents 100% of *Ot* in a single infected cell expressing the protein. At least 20 cells were assessed per replicate, and each experiment included three biological replicates.

Imaging was performed on a Nikon Eclipse Ti2-E Inverted Microscope (Nikon, Japan) equipped with a PLAN Apo Lambda 100× Oil (numeric aperture: 1.45) objective plus intermediate magnification switching to 1.5× on the main body. A total of 405 nm, 488 nm, 555 nm, and 647 nm filters were applied with a Hamamatsu ORCA-fusion Digital Camera C14440. *Z*-stack was performed using Define from top to bottom, followed by maximum intensity projection and 2D deconvolution.

Click labeling was based on the Click-iT HPG Alexa Fluor Protein Synthesis Assay Kit (Thermo Scientific) strategy as described previously (30). Briefly, L-15B300 medium was removed from ISE6 tick cells infected with *Ot* strain TA686 and replaced with minimal DMEM medium lacking L-methionine and FBS and containing 50 µM L-homopropargylglycine (HPG) for 6 h at 32°C. Bacteria were then washed and fixed with 4% PFA and labeled with primary and secondary antibodies as described above. After the last washing, the Click-iT reaction cocktail was supplemented, and cells were incubated in the dark for 1 h at room temperature. The azide dye Alexa Fluor 488 was used at a final concentration of 5 µM. The cells were imaged as above.

Statistical analysis

The statistical analyses were conducted using GraphPad Prism 11.0.0. Growth curves of *Ot* at various temperatures were compared using two-way analysis of variance (ANOVA) by Tukey's HSD test, while between strains using the unpaired *t*-test. The differences between protein expression levels were evaluated with Fisher's exact test. Data were presented as mean ± standard deviation.

RESULTS

Orientia tsutsugamushi replicates in tick cells

Tick cell lines share many physiological characteristics with the arthropods from which they were derived, and can grow at incubation temperatures between 28°C and 34°C (21). Previous studies have reported the optimal growth temperature for ISE6 and BME/CTVM23 at 32°C (31), which differs from 37°C used for most mammalian cell models. Based on this, we compared the growth of *Ot* at different temperatures to determine how temperature influences bacterial replication within tick cells (Fig. 1A). We compared the growth at optimal, i.e., 32°C, with suboptimal temperatures at 25°C and 35°C and determined that there was no significant difference in *Ot* growth at these different temperatures in either ISE6 or BME/CTVM23. Although both cell lines supported high bacterial loads, in ISE6, *Ot* reached the highest bacterial number at day 14 and in BME/CTVM23 at day 19 post-infection, which resulted in sudden host cell death shortly thereafter. The growth of the avirulent *Ot* strain TA686 was comparable to that of the virulent Karp strain at 32°C (Fig. S1). In both strains, more than 90% of cells were infected at late stages of infection, and a sudden pH change of the culture media could be observed through media color change, likely accounting for the rapid host cell death.

Downloaded from https://journals.asm.org/journal/aem on 12 June 2026 by 81.101.145.98.

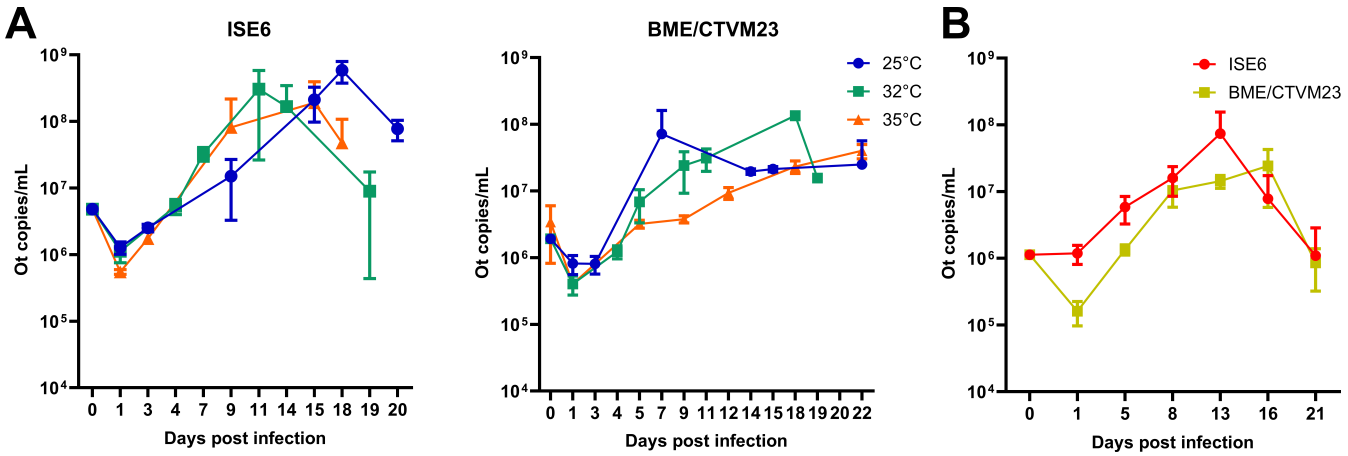


FIG 1 *Orientia tsutsugamushi* strains TA686 and Karp grow in tick cell lines. (A) Graphs showing bacterial copy number per mL of the *Ot* strain TA686 at 25°C, 32°C, and 35°C in ISE6 and BME/CTVM23 cell lines. (B) Bacterial copy number of the *Ot* strain Karp in ISE6 and BME/CTVM23 at 32°C. Bacterial load was measured by qPCR using primers against the conserved single-copy bacterial gene *tsa47*. Graph shows mean and standard deviation taken from three independent biological replicates. Statistical analysis was carried out using two-way ANOVA and showed no significant difference between TA686 growth at different temperatures for ISE6 or BME/CTVM23, nor between Karp growth in ISE6 compared with BME/CTVM23 ($P > 0.05$; ns).

Ot maintains a cytoplasmic location in tick cells

Ot, an intracellular pathogen that resides free in the cytoplasm without a host cell-derived vacuole (non-vacuolar), has been previously imaged in invertebrate tissues and mammalian cell lines (32, 33), but no imaging has been reported in arthropod cell lines. Arthropod cells represent a natural environment for vector-borne pathogens; hence, understanding *Ot* intracellular interactions in these cells is essential for unveiling its adaptation and transmission mechanisms. To investigate the *Ot* strain TA686 localization in arthropod cells, we conducted TEM and SEM imaging to characterize its intracellular distribution, morphology, and association with host cell structures. We focused on imaging late-stage infection to visualize *Ot* exit from host cells. TEM and SEM images of *Ot* in ISE6 and BME/CTVM23 cells revealed multiple *Ot* bacteria in the cytoplasm of tick cells that were not enveloped by a third membrane (Fig. 2). The bacteria were distributed throughout the host cell cytoplasm with no apparent localization to specific regions. Two membranes could be observed, as expected for this diderm bacterium, with the inner membrane appearing more electron dense than the outer membrane (Fig. 2). This is in contrast to reports of *Ot* in mite tissue in which electron-dense outer membrane and less-dense inner membrane were seen, although this may reflect differences in sample preparation (33). *Ot* in both tick cell lines measured approximately 0.5 µm in width and 2–4 µm in length and exhibit irregular morphologies. Moreover, in both cell lines, *Ot* appeared to bud off the host cell periphery, similar to its behavior in mammalian cells (33), acquiring a portion of the host plasma membrane during the process. Some *Ot* also displayed blebs, small vesicles formed by membraneous fragments at the bacterial surface (Fig. 2E), as seen in mammalian cells (34). Although the growth of *Ot* in BME/CTVM23 was somewhat slower than in ISE6 (Fig. 1), there was no difference in bacterial morphology between the two tick cell lines. These findings demonstrated that *Ot* retains its cytoplasmic location in tick cells and exits infected cells by budding.

The infection cycle of *Ot* in tick cells is characterized by temporal changes in expression of surface proteins

To explore the intracellular growth of *Ot* in tick cells, we performed a time-course infection of ISE6 and BME/CTVM23 cells with strain TA686. Immunofluorescence microscopy revealed that bacterial load increased progressively from 4 to 11 days post-infection in ISE6 and from 5 to 14 days post-infection in BME/CTVM23 (Fig. 3A through

Downloaded from https://journals.asm.org/journal/aem on 12 June 2026 by 81.101.145.98.

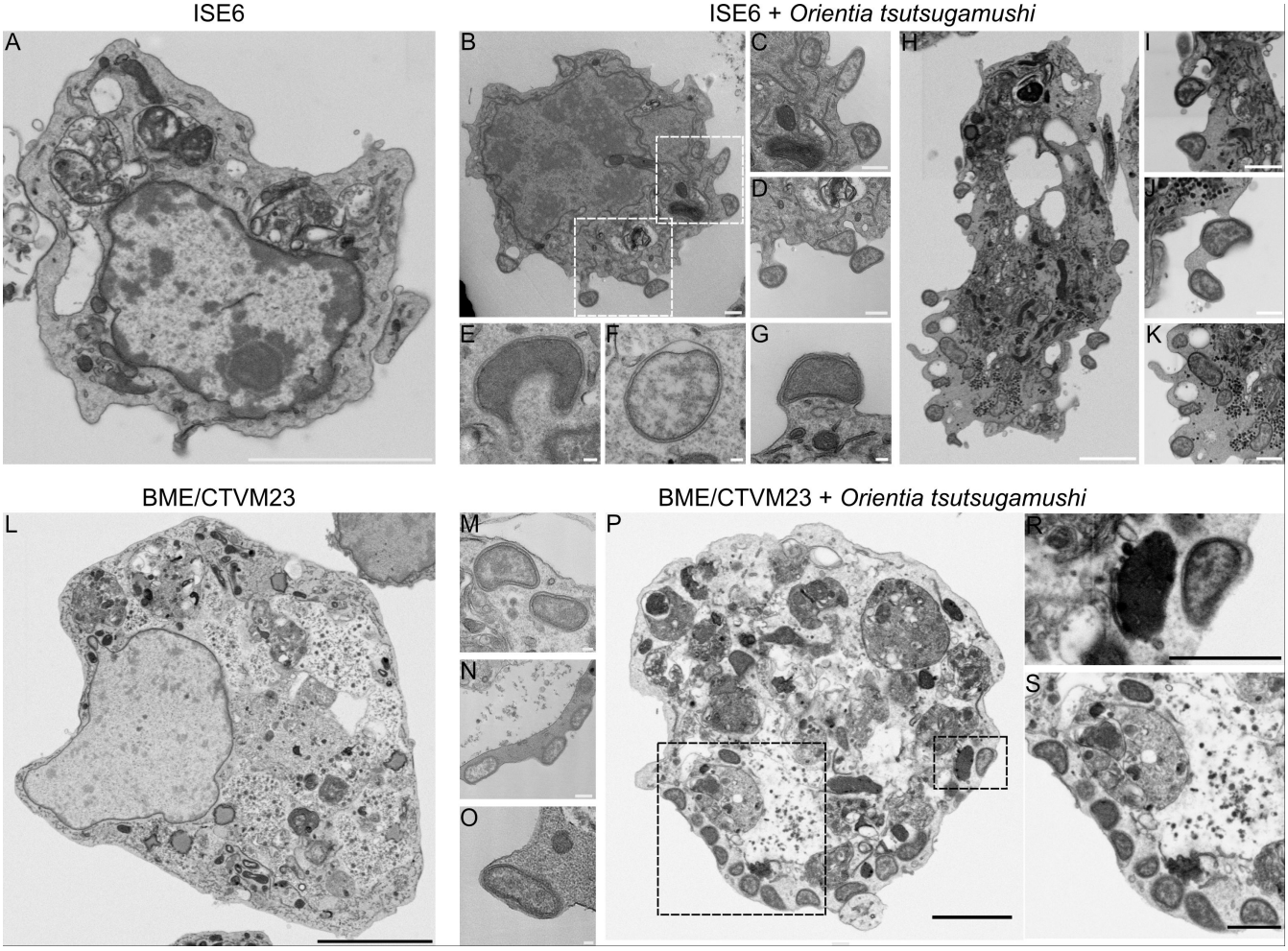


FIG 2 Morphological characterization of *Orientia tsutsugamushi* strain TA686 grown in tick cell lines. Transmission (A–G and L–O) and scanning (H–K and P–S) electron microscopy images of ISE6 (A–K) and BME/CTVM23 (L–S) tick cell lines, respectively, 11 and 19 days post inoculation with *Ot* strain TA686. (A) Image of an uninfected ISE6 cell; scale bar 500 nm. (B) Image of ISE6 cell infected with *Ot*; scale bar 500 nm. (C and D) Detailed images of *Ot* budding from the host cell; scale bar 500 nm. (E) Blebbing of an *Ot* cell; scale bar 100 nm. (F) Round morphology of *Ot* cell; scale bar 100 nm. (G) Budding *Ot*; scale bar 100 nM. (H) ISE6 cell infected with *Ot*; scale bar 500 nm. (I–K) Budding *Ot*; scale bar 100 nm. (L) Image of uninfected BME/CTVM23 cell; scale bar 200 nm. (M–O) Detailed images of *Ot* in BME/CTVM23; scale bars 100 nm, 500 nm, and 100 nm. (P) BME/CTVM23 cell infected with *Ot*; scale bar 500 nm. (R and S) Detailed images of *Ot*; scale bar 200 nm.

D). While most *Ot* strains localize to a tight perinuclear colony in mammalian cells, the avirulent strain TA686 is more dispersed throughout the cytoplasm (22). The subcellular localization of TA686 in tick cells resembled the previously described dispersed distribution. We used immunofluorescence microscopy to assess expression patterns of three surface proteins: TSA56, ScaA, and ScaC. All three proteins were detected on the surface of at least some bacteria at all time points. There was substantial heterogeneity in the levels of ScaA and ScaC proteins observed on individual bacteria within an infected cell. The patterns varied at different time points, with similar trends between the two tick cell lines. ScaC protein was detected especially during the early stages of infection (Fig. 3B and 3D and 3F), whereas ScaA protein levels increased as the infection progressed (Fig. 3A and 3C and 3E). At early stages of infection, bacteria expressing ScaA were scattered throughout the cell, while at late stages of infection, ScaA-positive bacteria were particularly prevalent at the cell periphery. While most bacteria had measurable levels of TSA56 protein at all stages of infection, a very small proportion of individual bacteria, only at the beginning of the infection, were observed with detectable ScaA but no

Downloaded from https://journals.asm.org/journal/aem on 12 June 2026 by 81.101.145.98.

TSA56, suggesting these two proteins may be differentially regulated during infection. Likewise, some host cells contained bacteria expressing ScaC but no detectable TSA56 at the early stage of infection. Moreover, we observed that the percentage of ScaC-expressing bacteria decreased more strongly in BME/CTVM23 compared to ISE6 cells (Fig. 3D and 3F). This temporal difference in expression patterns suggests that ScaC may play a role in early host cell interactions, while ScaA could be associated with a role in maintaining bacterial adhesion or replication. Together, these findings demonstrated that *Ot* TA686 replicates actively within tick cells and shows differential surface protein expression patterns during intracellular development.

Karp replicates in tick cells and shows a temporal shift from ScaC to ScaA expression

Ot strains differ in pathogenicity (22); therefore, we sought to analyze the intracellular lifecycle of the virulent Karp strain in ISE6 and BME/CTVM23 cells. Similar to the avirulent TA686 strain, *Ot* Karp readily infected and replicated within tick cells, with a consistent increase in the abundance of TSA56 between day 5 and day 9, indicating active intracellular replication of Karp in both cell lines (Fig. 1B). We explored the subcellular localization of Karp and expression of TSA56, ScaA, and ScaC proteins (Fig. 4). We found that Karp displayed stable ScaC expression in comparison to the patterns seen in TA686, and although the expression of TSA56/ScaC varied in certain cells, we found no significant difference in ScaC expression over time. However, we observed increasing ScaA expression over time in both ISE6 and BME/CTVM23. The patterns of ScaA gene expression between TA686 and Karp strains indicate that phase-specific regulation in the late stages of infection is conserved across phylogenetically distinct strains despite differences in pathogenicity. Furthermore, unlike reports from various mammalian cell lines, we did not observe the characteristic perinuclear colony formation even at 1 day post-infection (Fig. S2 and S3). Instead, the intracellular distribution of the Karp strain resembled that of TA686, with even dispersal throughout the host cell cytoplasm.

Microtubule disruption does not alter *Ot* localization in tick cells

Ot typically clusters into a tight perinuclear colony in infected mammalian cells, although it was recently shown that the avirulent strain TA686 is unusual in displaying this phenotype more weakly than other strains (22). It is known that the perinuclear trafficking in mammalian cells is mediated by the bacterial surface protein ScaC, which interacts with dynein via a BicD1/2 adapter to move along microtubule filaments (16). Nocodazole treatment, which disrupts microtubule filaments, has been shown to displace intracellular *Ot* from the perinuclear location in human and murine cells *in vitro* (16, 35). The observed lack of perinuclear localization of either Karp or TA686 *Ot* (Fig. 3 and Fig. 4 and Fig. S2) led us to ask whether microtubules play any role in the positioning of *Ot* in arthropod cells. To address this, we treated *Ot*-infected ISE6 cells with 10 µM nocodazole as used previously in HeLa cells (16) and assessed the impact on intracellular bacterial (IB) distribution (Fig. 5). While nocodazole clearly destabilizes and depolymerizes microtubules in ISE6 tick cells, as shown by a loss of β-tubulin labeling, there was no change in the spatial arrangement of *Ot* Karp. This indicates that *Ot* distribution in tick cells, unlike in mammalian cells, does not require intact microtubules.

ScaA expression correlates with decreased metabolic activity

Ot is an obligate intracellular bacterium with limited metabolic and biosynthetic capability, relying on host cells as sources of carbon, nitrogen, and essential metabolic intermediates (36). *Ot* exhibits distinct IB and EB populations, and previous studies showed that, unlike inactive EB, IB is translationally active at 5 days post-infection in mammalian cells (10). Our observations revealed an increased expression of the ScaA gene during the late stages of infection in tick cells, leading us to hypothesize that

Downloaded from https://journals.asm.org/journal/aem on 12 June 2026 by 81.101.145.98.

Downloaded from https://journals.asm.org/journal/aem on 12 June 2026 by 81.101.145.98.

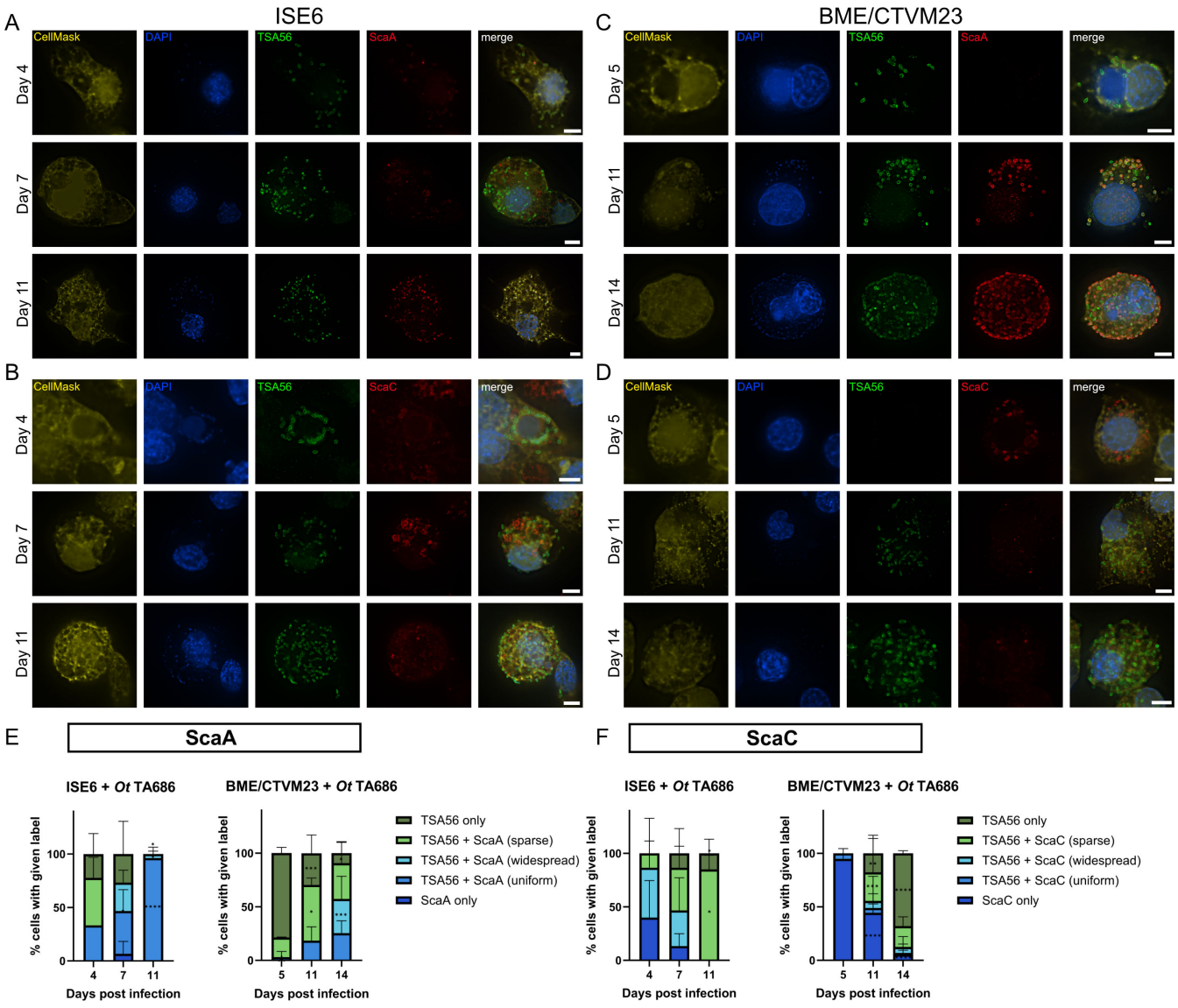


FIG 3 Analysis of the subcellular localization and expression of bacterial surface proteins TSA56, ScaA, and ScaC on *Orientia tsutsugamushi* strain TA686 at different times after infection in ISE6 and BME/CTVM23 cells. (A and B) Immunofluorescence microscopy images of *Ot* TA686 in ISE6 at 4, 7, and 11 days post-infection. The bacteria expressed the outer membrane proteins TSA56, ScaA (A), and ScaC (B).(C and D) Immunofluorescence microscopy images of *Ot* TA686 in BME/CTVM23 cells at 5, 11, and 14 days post-infection. Cytosol and nuclei were stained with CellMask and DAPI, respectively. Scale bars represent 5 µm. (E and F) Graphs showing quantification of data represented in panels A–D. Infected tick cells were scored as having bacteria inside them that were labeled with TSA56, ScaA, ScaC, or both. *Ot* was categorized into "Sparse" expression, where <50% *Ot* cells were TSA56, ScaA, or ScaC positive. Accordingly, "widespread" expression was assigned, where 50%–99% were positive, and "uniform" indicates that 100% of *Ot* in a single host cell expressed TSA56, ScaA, or ScaC. The data were obtained from three independent biological replicates. A minimum of 20 cells was counted per replicate. The graph shows the mean and standard deviation. Statistical analysis was carried out using a Fisher's exact test. Statistically significant differences in any one pattern between one time point compared to the one immediately preceding it are shown on the graphs. **P* ≤ 0.05, ****P* ≤ 0.001, and *****P* ≤ 0.0001.

ScaA-enriched bacteria are entering a maturation stage of growth in preparation for exit via budding. Since extracellular bacteria are metabolically inactive, we would expect that intracellular late-stage infection ScaA-positive bacteria would have decreased metabolic activity. To test this, we used a microscopy-based assay of protein synthesis activity using a clickable methionine analog L-HPG which is conjugated to a fluorophore following fixation (30).

The distribution of the *Ot* strain TA686 exhibiting different combinations of ScaA abundance and HPG incorporation at 11 days post-infection in ISE6 cells is shown in Fig.

Downloaded from https://journals.asm.org/journal/aem on 12 June 2026 by 81.101.145.98.

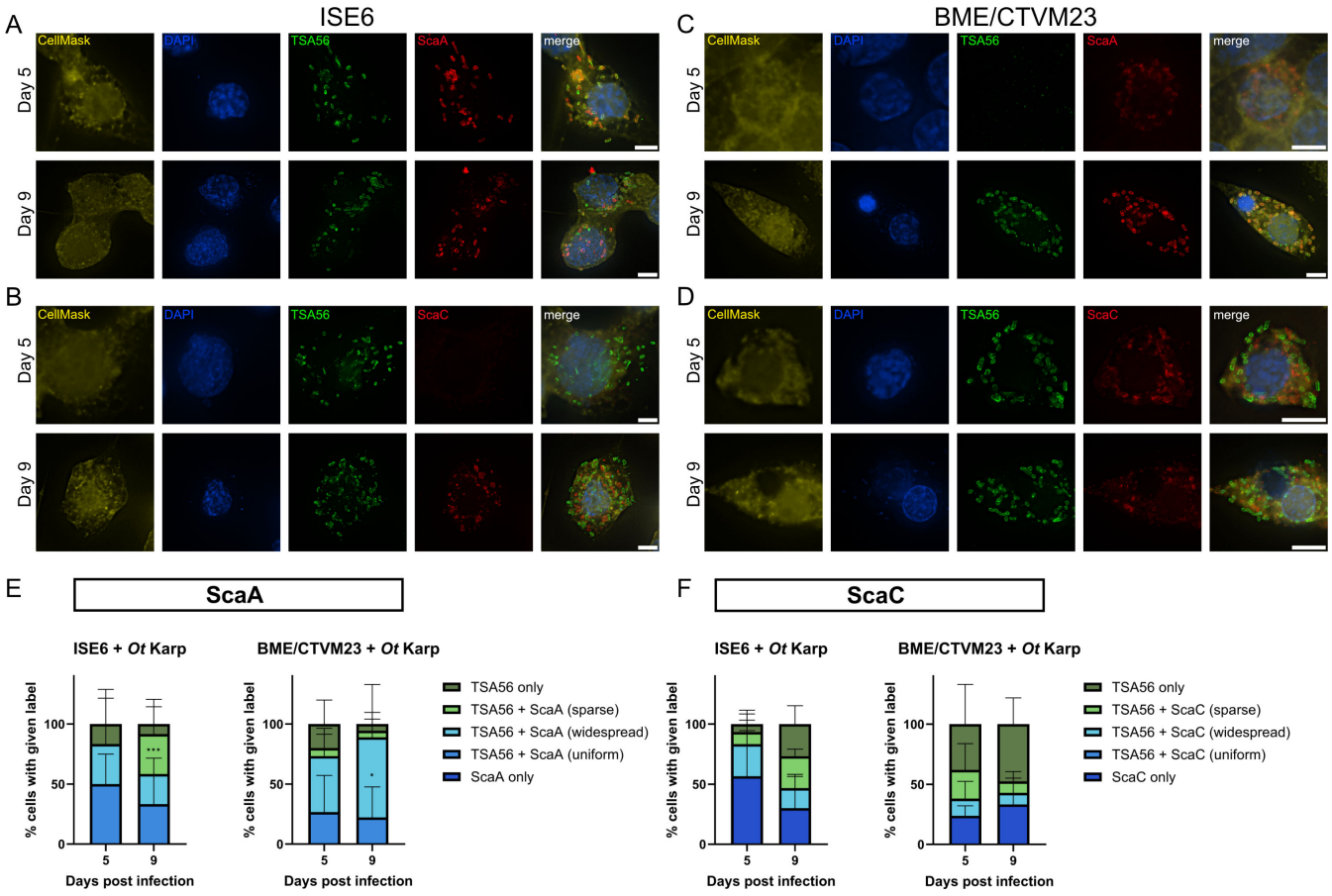


FIG 4 Analysis of the subcellular localization and expression of bacterial surface proteins TSA56, ScaA, and ScaC on *Orientia tsutsugamushi* strain Karp at different times after infection in ISE6 and BME/CTVM23 cells. (A–D) Immunofluorescence microscopy images of *Ot* Karp in ISE6 (A and B) and BME/CTVM23 (C and D) at 5 and 9 days post-infection. The bacteria expressed the outer membrane proteins TSA56 (green), ScaA (red; A and C), and ScaC (red; B and D). Cytosol (yellow) and nuclei (blue) were stained with CellMask and DAPI, respectively. Scale bars represent 5 µm, $N = 3$, $n = 20$. (E and F) Graphs showing quantification of data represented in panels A–D. Infected tick cells were scored as having bacteria inside them that were labeled with TSA56, ScaA, ScaC, or both. "Sparse" indicates <50%, "widespread" 50%–99% and "uniform" 100% of host cells with the given label. The data were obtained from three independent biological replicates, where a minimum of 20 cells were counted per replicate. The graph shows the mean and standard deviation. Statistical analysis was carried out using a Fisher's exact test. Statistically significant changes in any one pattern between day 9 and day 5 are shown on the graphs. $^{*}P \leq 0.05$ and $^{***}P \leq 0.001$.

6. As described above, TSA56 and ScaA were differentially present in different bacteria, but we additionally observed substantial variability in translation activity marked with HPG labeling. *Ot* displayed multiple phenotypic states, all expressing TSA56 but with ScaA levels ranging from sparse (<50% of ScaA-positive cells) to uniform (100% ScaA-positive cells). Notably, the bacteria lacking ScaA expression (Fig. 6B) still showed HPG incorporation. In contrast, bacteria with high ScaA abundance were metabolically inactive, exhibiting little to no HPG incorporation. Among the double-labeled populations, most ScaA-positive bacteria displayed only low-to-medium HPG incorporation. Together, these findings suggest an association between higher ScaA abundance and reduced protein biosynthesis, consistent with the possibility that ScaA-enriched bacteria represent a metabolically less active state that may occur during late stages of infection.

DISCUSSION

Under natural conditions, *Ot* is maintained in the *Leptotrombidium* mite population through transovarial transmission, with infection passing directly from females to their offspring. The chigger larvae thus emerge already carrying *Ot*, serving as the primary vectors responsible for transmitting the pathogen to vertebrate hosts. Although *Ot* has

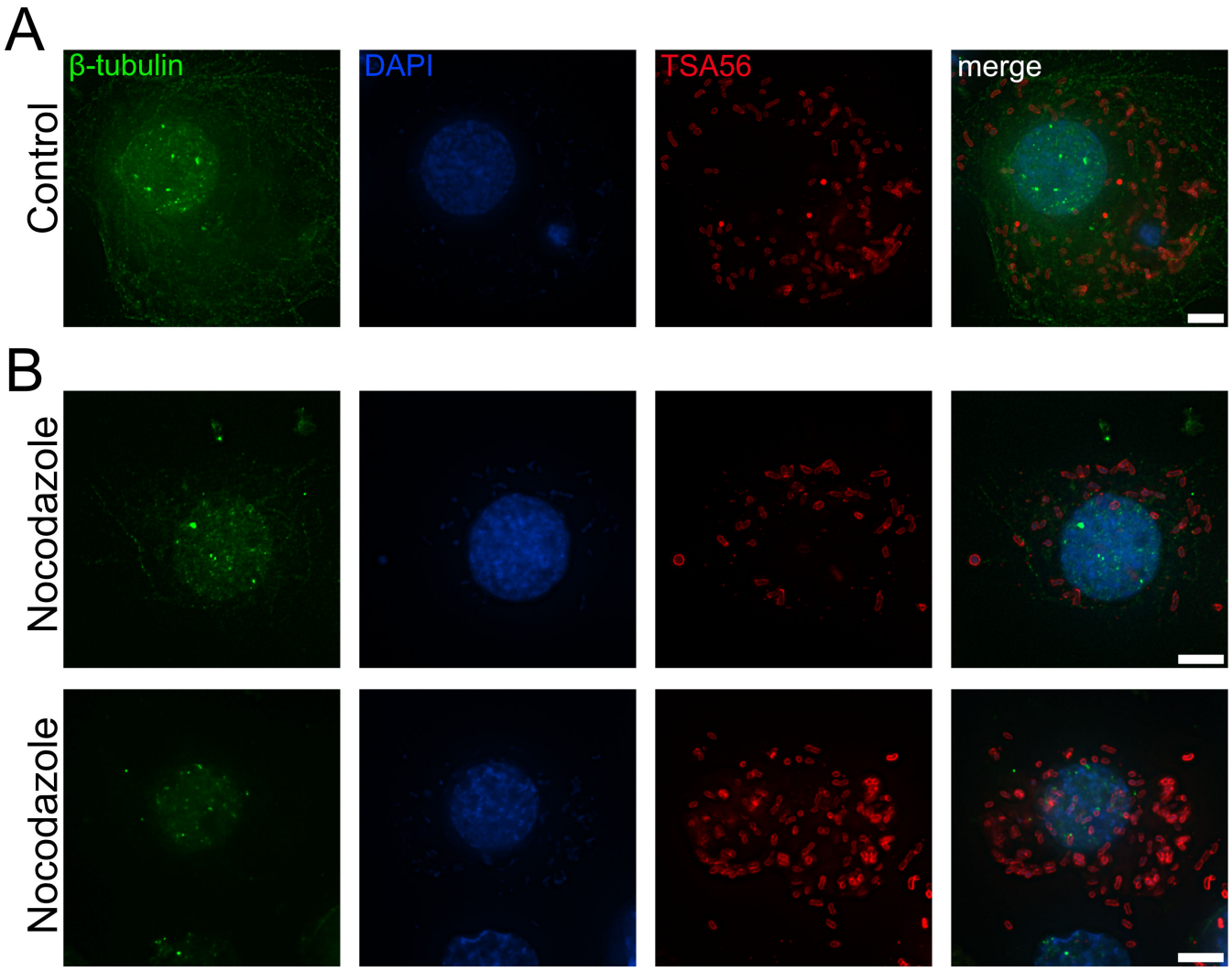


FIG 5 Nocodazole treatment does not alter the intracellular position of *Orientia tsutsugamushi* strain Karp in ISE6 cells. Immunofluorescence images of ISE6 cells at 11 days post-infection, treated with either (A) DMSO (control) or (B) 10 µM nocodazole. Karp was detected using an antibody against the outer membrane protein TSA56 (red); β-tubulin was stained with a primary antibody (green) and nuclei with DAPI (blue). The data were obtained from three independent biological replicates. A minimum of 20 cells were screened per replicate for either control or the nocodazole effect on *Ot* distribution. Scale bars represent 5 µm.

Downloaded from https://journals.asm.org/journal/aem on 12 June 2026 by 81.101.145.98.

been studied *in vivo* in infected mites and mice and *in vitro* in mammalian cell cultures (10, 22, 33), it has not been investigated in any arthropod cell culture system. In this context, our study has unveiled a novel arthropod model for studying this obligate intracellular bacterium, *Ot*, providing new opportunities to dissect vector-pathogen interactions in a controlled and tractable system.

Tick cell lines have an invaluable role in *in vitro* studies to investigate Rickettsiales bacteria. Numerous studies have demonstrated that several vector-borne pathogens can be successfully isolated, cultured, and propagated in tick cells, including bacterial species *Anaplasma phagocytophilum*, *Anaplasma marginale*, *Ehrlichia canis*, *Ehrlichia ruminantium*, *Rickettsia raoultii*, and a close relative of *Ot*, *Occidentia massiliensis* (21, 24, 31, 37–40). These systems have provided essential insights into pathogen replication dynamics, host cell responses, and mechanisms of vector competence. Likewise, they have also led to comparative studies across different Rickettsiales species, enabling the identification of intricate strategies that these obligate intracellular bacteria employ to survive within arthropod hosts (41, 42). Although *Ot* is a mite-borne bacterium, there are currently no mite-derived cell lines available. This limitation has created a major gap in our ability to dissect primary *Ot*-host interactions. In the absence of a homologous arthropod model,

Downloaded from https://journals.asm.org/journal/aem on 12 June 2026 by 81.101.145.98.

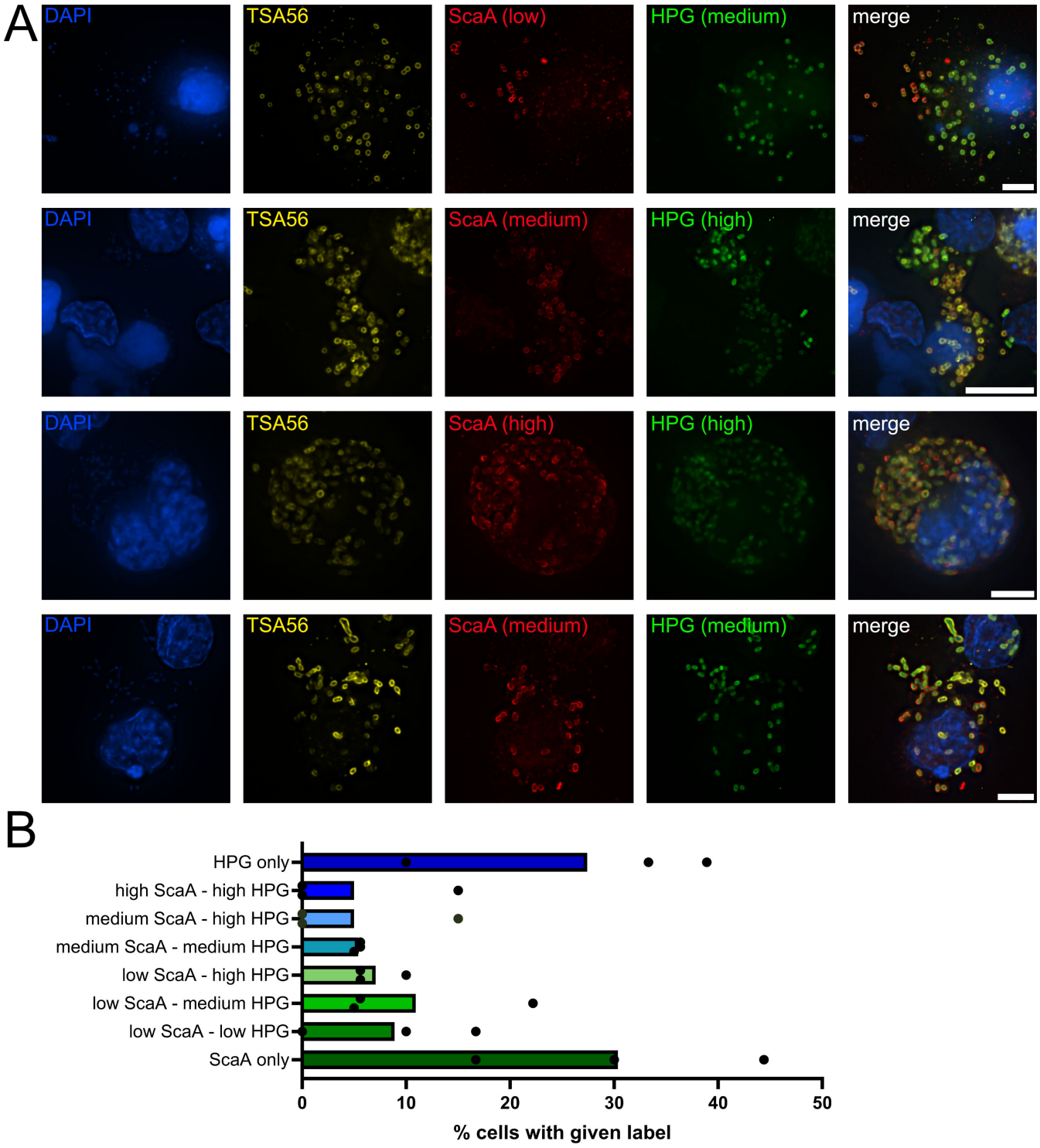


FIG 6 Analysis of the metabolic activity of individual intracellular *Orientia tsutsugamushi* strain TA686 bacteria reveals a negative correlation between ScaA expression and metabolic activity. (A) Immunofluorescence microscopy images of ISE6 cells infected with *Ot* TA686 at 11 days post-infection, showing examples of variable metabolic *Ot* profiles. *Ot* was labeled with the clickable methionine analog homopropargylglycine (HPG, green), antibodies against surface protein TSA56 (yellow) and ScaA (red). DNA (DAPI) is shown in blue. Scale bars represent 5 µm. (B) Quantification of metabolic activity, as measured by a detectable HPG incorporation, is shown as the percentage of *Ot*-infected cells falling into each category of combined ScaA abundance and HPG signal. High indicates cells with 100% of cells expressing the protein with a given label, medium 50%–99% of cells, and low <50% of cells. The bars represent mean and dots average score of individual replicates. The data were obtained from three independent biological replicates, where a minimum of 20 cells were counted per replicate.

Downloaded from https://journals.asm.org/journal/aem on 12 June 2026 by 81.101.145.98.

tick cell lines are an important tool for studying *Ot in vitro*. Tick cells share key innate immune pathways, endocytic processes, and intracellular trafficking machinery with other arthropods, making them valuable for studying how *Ot* invades, persists, and manipulates arthropod cells. In this study, we used two cell lines derived from different tick genera, *I. scapularis* ISE6 and *R. microplus* BME/CTVM23, to investigate *Ot* infection dynamics in arthropod cells.

The observed tick cell infection phenotype differed from that described in mammalian cells. *Ot* exhibited slower growth in both tick cell lines, which is consistent with expected differences in optimal replication temperature between arthropod and mammalian hosts. Interestingly, however, *Ot* growth was not affected by the range of temperatures we tested, namely 25°C–35°C. This observation suggests that *Ot* may possess a broad thermal tolerance or dynamic adaptive mechanisms that modulate replication independently of temperature variations. This is supported by a previous study on the *Ot* strain Okazaki, which exhibited better growth at 31°C than 36°C (43) in mammalian cells, indicating that some *Ot* strains may be intrinsically adapted to cooler conditions. In nature, *Ot* and many other Rickettsiales reside in ectothermic mites and ticks, where environmental temperature can fluctuate considerably. Such flexibility may represent an evolutionary adaptation that enables *Ot* to maintain stable infections within arthropod hosts despite highly variable thermal environments. Furthermore, strains TA686 and Karp showed similar overall infection dynamics in both tick cell lines, but TA686 consistently reached higher numbers than Karp in ISE6 cells. These differences indicate that TA686 replicates more efficiently in tick cells than Karp, suggesting strain-specific variation in adaptation to arthropod hosts.

While *Ot* exhibits apparent differences in its growth dynamics in tick cells, its overall morphology, cytoplasmic localization, and budding resemble the characteristics in mammalian cells (10, 44, 45). This similarity indicated that *Ot* maintains a stable intracellular lifestyle despite the physiological differences between the arthropod and mammalian hosts, highlighting its broad host adaptability.

Immunofluorescence microscopy using three bacterial surface proteins and microscopy of metabolically active cells using HPG labeling revealed heterogeneity in *Ot* populations over time and within individual infected cells. In mammalian cells, intracellular bacteria exhibit high levels of ScaA, and some metabolically inactive extracellular bacteria have high levels of ScaC protein (10). In tick cells, *Ot* showed high ScaC levels in early infections, whereas ScaA levels were higher at later stages. This substantial difference between patterns of Sca proteins between mammalian and arthropod cells indicates the unique adaptation of *Ot* to various hosts and sheds light on their interactions with the host. Furthermore, it was recently shown that the bacterial autotransporter protein ScaC in mammalian cells recruits dynein via adaptor proteins BICD1/2, driving microtubule-based movement (16). Here, we showed that *Ot* is almost always localized throughout the cytoplasm of tick cells rather than in a perinuclear cluster as seen in mammalian cells, and disrupting microtubules with nocodazole does not noticeably alter *Ot* localization in tick cells. Although we cannot entirely exclude any role for microtubule-dependent trafficking of *Ot* at different time points or under different conditions, our results suggest that ScaC-mediated trafficking may not be used in these cell lines. In addition, the higher levels of ScaC in the early-stage infection might reflect the introduction of ScaC-rich bacteria to tick cells, since prior to their infection, we propagated and harvested *Ot* in L929 at day 6 post-infection. By contrast, the increase in ScaA at late times after infection and in bacteria located at the surface of cells suggests a possible role for this protein in maturation and exit. This is supported by the observation that ScaA-positive bacteria at the surface of infected cells generally exhibited decreased translational activity as measured by HPG incorporation, although the substantial heterogeneity in these measurements demonstrates that additional levels of regulation are likely involved.

In summary, by establishing an arthropod cellular infection model for *Ot*, our study provides a critical tool for understanding how this obligate intracellular pathogen

interacts with its vector. Insights into the intracellular dynamics, host-specific gene regulation, and maturation processes of *Ot* can inform strategies to disrupt transmission from mites to humans, ultimately contributing to better prevention and control of scrub typhus. Moreover, understanding vector-borne pathogen biology in arthropod cells can guide the development of vaccines, addressing a significant global health threat.

ACKNOWLEDGMENTS

We thank the University of Minnesota for permission to use the ISE6 cell line and the Tick Cell Biobank at the University of Liverpool and Dr. Catherine Hartley for supplying both tick cell lines and training in their use. We thank the Electron Microscopy Facility of the Microscopy Bioscience Platform for their technical support and training on equipment use.

J.S. was supported by Wellcome Trust grant 224277/Z/21/Z. L.B.-S. was supported by the Wellcome Trust grant no. 223743/Z/21/Z.

AUTHOR AFFILIATIONS

[1]Cambridge Institute for Medical Research, University of Cambridge, Cambridge, United Kingdom
[2]Microscopy Bioscience Platform, School of Biological Sciences, University of Cambridge, Cambridge, United Kingdom
[3]Institute of Infection, Veterinary and Ecological Sciences, University of Liverpool, Liverpool, United Kingdom
[4]Department of Biochemistry, University of Cambridge, Cambridge, United Kingdom
[5]Department of Pathology, University of Cambridge, Cambridge, United Kingdom

AUTHOR ORCIDs

Magda A. Rogowska-van der Molen http://orcid.org/0000-0001-5910-4101
Jeanne Salje http://orcid.org/0000-0001-5802-4580

FUNDING

Funder	Grant(s)	Author(s)
Wellcome Trust	223743/Z/21/Z	Jeanne Salje

ADDITIONAL FILES

The following material is available online.

Supplemental Material

Supplemental material (AEM02540-25-s0001.pdf). Figures S1 to S3.

REFERENCES

1. Luce-Fedrow A, Lehman ML, Kelly DJ, Mullins K, Maina AN, Stewart RL, Ge H, John HS, Jiang J, Richards AL. 2018. A review of scrub typhus (*Orientia tsutsugamushi* and related organisms): then, now, and tomorrow. Trop Med Infect Dis 3:8. https://doi.org/10.3390/tropicalmed3010008
2. Khairkar M, Vagha S, Deotale V. 2023. Review on scrub typhus: an important etiology of acute undifferentiated fever illness. Cureus 15:e47290. https://doi.org/10.7759/cureus.47290
3. Xu G, Walker DH, Jupiter D, Melby PC, Arcari CM. 2017. A review of the global epidemiology of scrub typhus. PLoS Negl Trop Dis 11:e0006062. https://doi.org/10.1371/journal.pntd.0006062
4. Bonell A, Lubell Y, Newton PN, Crump JA, Paris DH. 2017. Estimating the burden of scrub typhus: a systematic review. PLoS Negl Trop Dis 11:e0005838. https://doi.org/10.1371/journal.pntd.0005838
5. Wang Q, Ma T, Ding F, Lim A, Takaya S, Saraswati K, Sartorius B, Day NPJ, Maude RJ. 2024. Global and regional seroprevalence, incidence, mortality of, and risk factors for scrub typhus: a systematic review and meta-analysis. Int J Infect Dis 146:107151. https://doi.org/10.1016/j.ijid.2024.107151
6. Izzard L, Fuller A, Blacksell SD, Paris DH, Richards AL, Aukkanit N, et al. 2010. Isolation of a novel *Orientia* species (O. chuto sp. nov.) from a patient infected in Dubai. J Clin Microbiol 48:4404–4409. https://doi.org/10.1128/JCM.01526-10
7. Weitzel T, Dittrich S, López J, Phuklia W, Martinez-Valdebenito C, Velásquez K, Blacksell SD, Paris DH, Abarca K. 2016. Endemic scrub typhus in South America. N Engl J Med 375:954–961. https://doi.org/10.1056/NEJMoa1603657
8. Abarca K, Martínez-Valdebenito C, Angulo J, Jiang J, Farris CM, Richards AL, Acosta-Jamett G, Weitzel T. 2020. Molecular description of a novel

Downloaded from https://journals.asm.org/journal/aem on 12 June 2026 by 81.101.145.98.

Downloaded from https://journals.asm.org/journal/aem on 12 June 2026 by 81.101.145.98.

orientia species causing scrub typhus in Chile. Emerg Infect Dis 26:2148–2156. https://doi.org/10.3201/eid2609.200918
9. Salje J. 2021. Cells within cells: *Rickettsiales* and the obligate intracellular bacterial lifestyle. Nat Rev Microbiol 19:375–390. https://doi.org/10.1038/s41579-020-00507-2
10. Atwal S, Wongsantichon J, Giengkam S, Saharat K, Pittayasathornthun YJ, Chuenklin S, Wang LC, Chung T, Huh H, Lee S-H, Sobota RM, Salje J. 2022. The obligate intracellular bacterium *Orientia tsutsugamushi* differentiates into a developmentally distinct extracellular state. Nat Commun 13:3603. https://doi.org/10.1038/s41467-022-31176-9
11. Kim MJ, Kim MK, Kang JS. 2013. Involvement of lipid rafts in the budding-like exit of *Orientia tsutsugamushi*. Microb Pathog 63:37–43. https://doi.org/10.1016/j.micpath.2013.06.002
12. Wongsantichon J, Jaiyen Y, Dittrich S, Salje J. 2020. *Orientia tsutsugamushi*. Trends Microbiol 28:780–781. https://doi.org/10.1016/j.tim.2020.02.014
13. Chu H, Lee JH, Han SH, Kim SY, Cho NH, Kim IS, et al. 2006. Exploitation of the endocytic pathway by *Orientia tsutsugamushi* in nonprofessional phagocytes. Infect Immun 74:4246–4253. https://doi.org/10.1128/IAI.01620-05
14. Giengkam S, Kullapanich C, Wongsantichon J, Adcox HE, Gillespie JJ, Salje J. 2023. *Orientia tsutsugamushi:* analysis of the mobilome of a highly fragmented and repetitive genome reveals ongoing lateral gene transfer in an obligate intracellular bacterium. mSphere:8:e00268-23.. https://doi.org/10.1128/msphere.00268-23
15. Sanchez SE, Chiarelli TJ, Park MA, Carlyon JA. 2024. *Orientia tsutsugamushi* infection reduces host gluconeogenic but not glycolytic substrates. Infect Immun 92:e0028424. https://doi.org/10.1128/iai.00284-24
16. Manigrasso G, Saharat K, Chaichana P, Kullapanich C, Atwal S, Boulanger J, Morgan TE, Kramer H, Salje J, Carter AP. 2025. The intracellular bacterium *Orientia tsutsugamushi* uses the autotransporter ScaC to activate BICD adaptors for dynein-based motility. Nat Commun 16:6122. https://doi.org/10.1038/s41467-025-61105-5
17. Rikihisa Y, Ito S. 1980. Localization of electron-dense tracers during entry of *Rickettsia tsutsugamushi* into polymorphonuclear leukocytes. Infect Immun 30:231–243. https://doi.org/10.1128/iai.30.1.231-243.1980
18. Ge Y, Rikihisa Y. 2011. Subversion of host cell signaling by *Orientia tsutsugamushi*. Microbes Infect 13:638–648. https://doi.org/10.1016/j.micinf.2011.03.003
19. Duh D, Punda-Polic V, Avsic-Zupanc T, Bouyer D, Walker DH, Popov VL, et al. 2010. *Rickettsia hoogstraalii* sp. nov., isolated from hard- and soft-bodied ticks. Int J Syst Evol Microbiol 60:977–984. https://doi.org/10.1099/ijs.0.011049-0
20. Bell-Sakyi L, Zweygarth E, Blouin EF, Gould EA, Jongejan F. 2007. Tick cell lines: tools for tick and tick-borne disease research. Trends Parasitol 23:450–457. https://doi.org/10.1016/j.pt.2007.07.009
21. Bell-Sakyi L. 2004. *Ehrlichia ruminantium* grows in cell lines from four ixodid tick genera. J Comp Pathol 130:285–293. https://doi.org/10.1016/j.jcpa.2003.12.002
22. Chaichana P, Satapoomin N, Kullapanich C, Chuenklin S, Mohammad A, Inthawong M, Ball EE, Burke TP, Sunyakumthorn P, Salje J. 2025. Comparative virulence analysis of seven diverse strains of *Orientia tsutsugamushi* reveals a multifaceted and complex interplay of virulence factors responsible for disease. PLoS Pathog 21:e1012833. https://doi.org/10.1371/journal.ppat.1012833
23. Kurtti TJ, Munderloh UG, Andreadis TG, Magnarelli LA, Mather TN. 1996. Tick cell culture isolation of an intracellular prokaryote from the tick Ixodes scapularis. J Invertebr Pathol 67:318–321. https://doi.org/10.1006/jipa.1996.0050
24. Alberdi MP, Nijhof AM, Jongejan F, Bell-Sakyi L. 2012. Tick cell culture isolation and growth of *Rickettsia raoultii* from Dutch *Dermacentor reticulatus* ticks. Ticks Tick Borne Dis 3:349–354. https://doi.org/10.1016/j.ttbdis.2012.10.020
25. Munderloh UG, Jauron SD, Fingerle V, Leitritz L, Hayes SF, Hautman JM, Nelson CM, Huberty BW, Kurtti TJ, Ahlstrand GG, Greig B, Mellencamp MA, Goodman JL. 1999. Invasion and intracellular development of the human granulocytic ehrlichiosis agent in tick cell culture. J Clin Microbiol 37:2518–2524. https://doi.org/10.1128/JCM.37.8.2518-2524.1999
26. Bell-Sakyi L. 1991. Continuous cell lines from the tick *Hyalomma anatolicum anatolicum*. J Parasitol 77:1006–1008. https://doi.org/10.2307/3282757
27. Giengkam S, Blakes A, Utsahajit P, Chaemchuen S, Atwal S, Blacksell SD, et al. 2015. Improved quantification, propagation, purification and storage of the obligate intracellular human pathogen *Orientia tsutsugamushi*. PLoS Negl Trop Dis 9:e0004009. https://doi.org/10.1371/journal.pntd.0004009
28. Weaver CM, Makdissi S, Di Cara F. 2022. Modified protocol for culturing *Drosophila* S2 R+ cells and adult plasmatocytes to study actin cytoskeleton dynamics. STAR Protoc 3:101588. https://doi.org/10.1016/j.xpro.2022.101588
29. Salje J. 2025. Quantifying *Orientia tsutsugamushi* and other Rickettsiales bacteria by real time qPCR v1. Protocols.io. https://doi.org/10.17504/protocols.io.8epv5nz4jv1b/v1
30. Atwal S, Giengkam S, Jaiyen Y, Feaga HA, Dworkin J, Salje J. 2020. Clickable methionine as a universal probe for labelling intracellular bacteria. J Microbiol Methods 169:105812. https://doi.org/10.1016/j.mimet.2019.105812
31. Ferrolho J, Simpson J, Hawes P, Zweygarth E, Bell-Sakyi L. 2016. Growth of *Ehrlichia canis*, the causative agent of canine monocytic ehrlichiosis, in vector and non-vector ixodid tick cell lines. Ticks Tick Borne Dis 7:631–637. https://doi.org/10.1016/j.ttbdis.2016.01.013
32. Atwal S, Chuenklin S, Bonder EM, Flores J, Gillespie JJ, Driscoll TP, Salje J. 2021. Discovery of a diverse set of bacteria that build their cell walls without the canonical peptidoglycan polymerase aPBP. mBio 12:e0134221. https://doi.org/10.1128/mBio.01342-21
33. Kadosaka T, Kimura E. 2003. Electron microscopic observations of *Orientia tsutsugamushi* in salivary gland cells of naturally Infected *Leptotrombidium pallidum* larvae during feeding. Microbiol Immunol 47:727–733. https://doi.org/10.1111/j.1348-0421.2003.tb03442.x
34. Paris DH, Phetsouvanh R, Tanganuchitcharnchai A, Jones M, Jenjaroen K, Vongsouvath M, Ferguson DPJ, Blacksell SD, Newton PN, Day NPJ, Turner GDH. 2012. Orientia tsutsugamushi in human scrub typhus eschars shows tropism for dendritic cells and monocytes rather than endothelium. PLoS Negl Trop Dis 6:e1466. https://doi.org/10.1371/journal.pntd.0001466
35. Kim SW, Ihn KS, Han SH, Seong SY, Kim IS, Choi MS. 2001. Microtubule- and dynein-mediated movement of *Orientia tsutsugamushi* to the microtubule organizing center. Infect Immun 69:494–500. https://doi.org/10.1128/IAI.69.1.494-500.2001
36. Min CK, Yang JS, Kim S, Choi MS, Kim IS, Cho NH. 2008. Genome-based construction of the metabolic pathways of *Orientia tsutsugamushi* and comparative analysis within the *Rickettsiales* order. Comp Funct Genomics 2008:623145. https://doi.org/10.1155/2008/623145
37. Blouin EF, de la Fuente J, Garcia-Garcia JC, Sauer JR, Saliki JT, Kocan KM. 2002. Applications of a cell culture system for studying the interaction of *Anaplasma marginale* with tick cells. Anim Health Res Rev 3:57–68.
38. Alberdi P, Ayllón N, Cabezas-Cruz A, Bell-Sakyi L, Zweygarth E, Stuen S, de la Fuente J. 2015. Infection of Ixodes spp. tick cells with different Anaplasma phagocytophilum isolates induces the inhibition of apoptotic cell death. Ticks Tick Borne Dis 6:758–767. https://doi.org/10.1016/j.ttbdis.2015.07.001
39. Shpynov SN, Fournier PE, Pozdnichenko NN, Gumenuk AS, Skiba AA. 2018. New approaches in the systematics of *Rickettsiae*. New Microbes New Infect 23:93–102. https://doi.org/10.1016/j.nmni.2018.02.012
40. Mediannikov O, Nguyen TT, Bell-Sakyi L, Padmanabhan R, Fournier PE, Raoult D. 2014. High quality draft genome sequence and description of *Occidentia massiliensis* gen nov., sp. nov., a new member of the family *Rickettsiaceae*. Stand Genomic Sci 9:9. https://doi.org/10.1186/1944-3277-9-9
41. Bui DC, Luo T, McBride JW. 2023. Type 1 secretion system and effectors in *Rickettsiales*. Front Cell Infect Microbiol 13:1175688. https://doi.org/10.3389/fcimb.2023.1175688
42. SchonME, Martijn J, Vosseberg J, KostlbacherS, Ettema TJG. 2022. The evolutionary origin of host association in the *Rickettsiales*. Nat Microbiol 7:1189–1199. https://doi.org/10.1038/s41564-022-01169-x
43. Tamura A, Makisaka Y, Enatsu T, Urakami H, Okubo K, Fukuhara M, Mahara F. 1999. Isolation of Orientia tsutsugamushi from patients in Shikoku and finding of a strain which grows preferentially at low temperatures. Microbiol Immunol 43:979–981. https://doi.org/10.1111/j.1348-0421.1999.tb03359.x
44. Ro HJ, Lee H, Park EC, Lee CS, Il Kim S, Jun S. 2018. Ultrastructural visualization of *Orientia tsutsugamushi* in biopsied eschars and monocytes from scrub typhus patients in South Korea. Sci Rep 8:17373. https://doi.org/10.1038/s41598-018-35775-9
45. Lee SM, Kwon HY, Im JH, Baek JH, Kang JS, Lee JS. 2015. Identification of outer membrane vesicles derived from *Orientia tsutsugamushi*. J Korean Med Sci 30:866–870. https://doi.org/10.3346/jkms.2015.30.7.866